atmosphere

Article

Eight-Day Typhoon Quantitative Precipitation Forecasts in Taiwan by the 2.5 km CReSS Model, Part II: Reduced Control of Track Errors on Rainfall Prediction Quality for Typhoons Associated with Southwesterly Flow

Chung-Chieh Wang [1,*], Wei-Kuo Soong [2], Chih-Wei Chien [1], Chih-Sheng Chang [1] and Shin-Yi Huang [1]

1 Department of Earth Sciences, National Taiwan Normal University, Taipei 11677, Taiwan; moneyj199328@gmail.com (C.-W.C.); shurin.chang@gmail.com (C.-S.C.); hshinyi0828@gmail.com (S.-Y.H.)
2 Department of Military Meteorology, Airforce Institute of Technology, Kaohsiung 820009, Taiwan; t094031@afats.khc.edu.tw
* Correspondence: cwang@ntnu.edu.tw

Abstract: Due to the enhancement by its steep mesoscale topography, the overall rainfall amount and distribution in Taiwan from typhoons, to a first degree, are determined by the storm track relative to the island. Therefore, the quality of typhoon quantitative precipitation forecasts (QPFs) from numerical models is often controlled by track errors, with better quality from those with smaller track errors. However, the present work demonstrates that in daily QPFs over Taiwan made by a cloud-resolving model during five seasons of 2012–2016, targeted for 84 days during 27 typhoons and at ranges of day one (0–24 h) to day eight (168–192 h), the control of track errors on QPF quality is reduced for typhoons associated with southwesterly flow, compared to those without, and decent QPFs could still be obtained with large track errors in some cases. Subsequently, the circumstances and reasons for good (or bad) QPFs in selected examples are further investigated to deepen our understanding of typhoon QPFs in Taiwan. Some common ingredients are found in three cases where good QPFs were produced at a longer range (day 7 or 8) without a good track: these typhoons passed near northern Taiwan and the southwesterly flow prevailed over much of the island during the accumulation period. Responsible for much of the rainfall in Taiwan, the southwesterly flow was reasonably captured, resulting in good QPFs. In another example where the typhoon moved across southern Taiwan, on the contrary, the rainfall was produced by the storm's circulation, and the QPF was degraded without a good enough track prediction.

Keywords: quantitative precipitation forecast (QPF); typhoon; cloud-resolving model; similarity skill score; categorical statistics; Taiwan

Citation: Wang, C.-C.; Soong, W.-K.; Chien, C.-W.; Chang, C.-S.; Huang, S.-Y. Eight-Day Typhoon Quantitative Precipitation Forecasts in Taiwan by the 2.5 km CReSS Model, Part II: Reduced Control of Track Errors on Rainfall Prediction Quality for Typhoons Associated with Southwesterly Flow. *Atmosphere* **2023**, *14*, 1047. https://doi.org/10.3390/atmos14061047

Academic Editor: Stephan Havemann

Received: 26 May 2023
Revised: 13 June 2023
Accepted: 16 June 2023
Published: 18 June 2023

1. Introduction

Located along one of the main paths of tropical cyclones (TCs) or typhoons in the western North Pacific (WNP), Taiwan is frequently hit by these storms roughly 3–5 per season [1]. Due to the steep mountains of the island, with the highest peak reaching 3952 m, rainfall from TCs as well as other organized convective systems are often considerably enhanced, e.g., [2–5], and consequently cause hazards such as inundation, floods, and landslides, and damage properties and infrastructure, e.g., [6]. To cope with the heavy rainfall brought by typhoons and reduce their impacts, quantitative precipitation forecasts (QPFs) using numerical models, e.g., [7,8], are in high demand in Taiwan. The performance of model QPFs is also constantly evaluated in order to improve their accuracy, lead time for warning and preparation, and probability estimates from the ensemble, e.g., [9–13].

Owing to the topographic effect mentioned above, it has long been recognized that when hit by a TC, the overall rainfall pattern over Taiwan at a given time is strongly controlled by the location of the storm relative to the island [14–16], with other factors such as the size and intensity of the TC playing a secondary role. As such, the total rainfall produced by a typhoon in Taiwan is often closely linked to its track near the island during the warning period, and there are nine main track types used for classification by the Central Weather Bureau (CWB) of Taiwan (Figure 1). Based on the above concept, a climatology model was developed by Lee et al. [17] to predict the total TC rainfall in Taiwan, given a projected track, using rainfall climatology observed by the dense network of automated rain gauges (further details on the data in Section 2.1) from past events. Later, ref. [18] improved their model by separating the climatology into those for two different basic track directions: westward-moving and northward-moving TCs. Applying a similar idea but using lagged ensemble predictions every 6 h from a suite of 5 km model members, Hong et al. [19] developed the Ensemble Typhoon QPF (ETQPF) system at the CWB. In this method, all predictions covering the target TCs were used as input data, such that both the stochastic nature of the model predictions, e.g., [20,21], and the specific characteristics of the target TCs can be taken into account. In the above and many other studies, an accurate track prediction is viewed as a prerequisite for a good model QPF, and the latter cannot be achieved without the former.

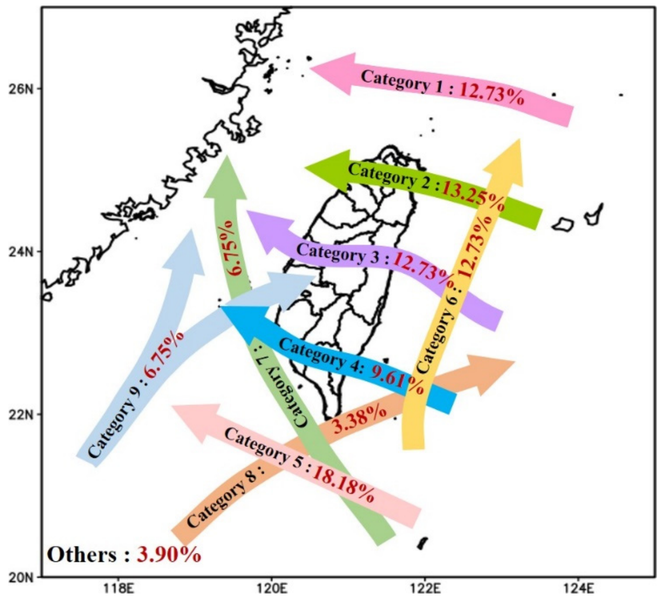

Figure 1. Schematic of CWB track types of typhoons invading Taiwan and their percentages (%). (Reproduced from CWB typhoon encyclopedia: https://www.cwb.gov.tw/V8/E/K/Encyclopedia/typhoon/, accessed on 28 March 2023).

As computer technology continues to advance, it has also been established in Taiwan during the past decade or so that more accurate typhoon heavy-rainfall QPFs can be obtained using higher model resolutions, e.g., [13,22–24], among other methods. Many studies have reported better and more realistic TC QPF results using a horizontal grid spacing (Δx) of 1–4 km and an adequate size for the fine domain, both for Taiwan [5,22,25–28] and in other regions [29–32]. For example, long-term results through multiple seasons in 2010–2015 using the Cloud-Resolving Storm Simulator (CReSS; Refs. [33,34]) at Δx = 2.5 km show improvements in typhoon QPFs within the short range (72 h), especially for the more rainy TC cases in Taiwan [13,24].

To both extend QPF results comparable to the above into longer lead times and obtain ensemble information without compromising model resolution, Wang et al. [35] further experimented on the time-lagged strategy, a method previously adopted by some researchers [36–39]. Different from these earlier attempts that applied the lagged method only at the short range (as in [19]), the 2.5 km CReSS was run once per day at 0000 UTC (since 2012) out to a range of eight days (192 h) in [35], since TCs typically have a relatively long lifespan of 1–2 weeks. Thus far, the time-lagged runs have also been carried out at 6 h intervals (four times per day) for some typhoons and were shown to be capable of providing both high-quality QPFs within the short range as well as a wide range of rainfall scenarios in Taiwan associated with different TC tracks at longer lead times [35,40]. For some TCs where the worse-case scenario turned out to occur, such as typhoons (TYs) Saola (2012), Matmo (2014), and Soudelor (2015), the particular scenario was successfully predicted almost one week before landfall, providing long lead times for preparation [41,42]. However, decent QPFs were only obtainable within a short range in some other cases [5,43] because the predictability varies among different TC cases.

Recently, the long-term performance of QPFs in daily time-lagged CReSS runs since 2012 over five seasons from 2012 to 2016, targeted for a total of 84 days covering the warning periods of 27 TCs, was also evaluated by Wang et al. [44], which is Part I of this study. Using objective skill scores (to be described in Section 2.4), the overall results within the short range (days 1–3) are close to and slightly better than those obtained earlier in [13,24], with better skill at shorter lead times, as expected (also [45]). At lead times beyond 72 h, decent QPFs that resemble the observation could still be produced for some target days if and when the track error was small in most cases. For the 14 TCs with a peak daily rainfall of $\geq$350 mm, such QPFs occurred the earliest, on average, around day 5. However, in [44] QPFs with high skill could still be obtained when the track errors of TCs were quite large on some occasions. This apparent low correlation between track errors and the quality of QPFs in some circumstances implies reduced control of the former over the latter. Specially, our first goal is to show that a major circumstance where the relationship between QPF quality and track error is weakened occurs in TCs that are associated with low-level southwesterly flow, through a statistical analysis of forecasts during the 2012–2016 seasons (Section 3), so these types of TCs are the main focus of this study. Then, as the second goal, several TC examples were further selected to investigate the circumstances and reasons for such a reduction in control and how good QPFs are still obtainable without a good track (Sections 4 and 5). Such aspects of typhoon QPFs in Taiwan have neither been noted nor investigated before.

The remaining part of this paper is arranged as described below. Section 2 describes the data, model, experiments, and methodology for QPF verification. In Section 3, a statistical analysis is presented to demonstrate the reduced control of track errors on the quality of QPFs in TCs that are associated with southwesterly flow. Four TC cases are selected, and their QPFs are discussed through examples in Section 4. In Section 5, further discussion is given, and finally we offer the concluding remarks in Section 6.

2. Data and Methodology

As a companion study, most of the data used here are the same as those in [44,45], which perform long-term verification of CReSS forecasts (also [13,24] for short-range forecasts). The common data include model forecast data and most of the observational data. Therefore, these data and the related methodology will only be briefly described below, and readers are referred to earlier studies for further details.

2.1. Observational Data

The observational data utilized in this study included the following: The best-track data from the CWB were used for the calculation of model track errors. For synoptic discussion of selected examples, the National Centers for Environmental Prediction (NCEP) Global Forecast System (GFS) final analyses ($1^\circ \times 1^\circ$, every 6 h) were used, and those at 850 hPa are shown. To illustrate the rainfall scenarios in the model, they were compared with Precipitation Radar (PR) and/or Thematic Mapping Imager (TMI) observations from the Tropical Rainfall Measuring Mission (TRMM) satellites at selected times, available from the Naval Research Laboratory (NRL). For the verification of model QPFs in Taiwan, hourly data from the network of automated rain gauges operated by the CWB were used [46] and summed into daily values for the target periods. During 2012–2016, the number of gauge sites varied between 433 and 523, with an average number of 480. To perform verification, model results were interpolated onto the gauge sites available in the target periods, regardless of the skill measure adopted, as in [44].

2.2. The CReSS Model and Forecast Data

In this study, the CReSS model [33,34] was used. The model configuration remained the same during 2012–2016, with a horizontal grid spacing (Δx) of 2.5 km and dimensions of 744 × 544 with 40 levels, giving a domain size of 1860 km × 1360 km (Table 1). As a cloud model, all clouds are treated explicitly in CReSS, and the bulk cold-rain scheme [47–51] with six water species (vapor, cloud water, cloud ice, rain, snow, and graupel) is adopted. Other parameterized processes include turbulent mixing [34,52] and radiation and energy/momentum fluxes at the surface [53–55]. Using the NCEP GFS gross analyses and forecasts [56,57] as initial and boundary conditions (IC/BCs), the CReSS forecasts were made once per day at 0000 UTC in real time (Table 1), each with a range of eight days (192 h). Note here that the GFS gross analyses were produced in real time, and thus, were slightly different from the final analyses described earlier. In summary, the model data were the same as those described in [35,44].

Table 1. Domain configuration and cloud microphysics of the CReSS model in this study.

Grid spacing * (km; x, y, z)	$2.5 \times 2.5 \times 0.2-0.663$ (0.5)
Grid dimension	$744 \times 544 \times 40$
Domain size (km)	$1860 \times 1360 \times 20$
Forecast range and frequency	192 h and once daily (at 0000 UTC)
IC/BCs (including SST)	NCEP GFS analyses and forecasts ($1^\circ \times 1^\circ$, 26 levels)
Topography data	Real at $(1/120)^\circ$ resolution
Cloud microphysics	Bulk cold-rain scheme (six species)

* The vertical grid spacing (Δz) of CReSS is stretched and the smallest is at the bottom, and the parentheses give the averaged value.

2.3. Typhoon Cases and Target Days

During 2012–2016, a total of 27 typhoons occurred, for which the CWB issued warnings. There were 84 days (0000–2400 UTC) to cover all these warning periods, and they are the targets for the QPF evaluation, as given in Table 2 of [44]. For each target day, the model QPFs made on successive days, from the earliest one at the longest range (on day 8, i.e., 168–192 h) to the last one at the shortest range (on day 1 or 0–24 h), were examined. Since the focus of our Part II study here is on the control of track errors over the quality of QPFs in Taiwan for TCs associated with southwesterly flow, only those forecasts where the typhoon of interest remained strong enough and inside the model domain (i.e., its center identifiable) were included for analysis, accounting for 411 QPFs of 24 h periods. The results of the statistical analysis are presented in Section 3.

2.4. Verification of Model QPFs

The similarity skill score (SSS) recently defined and used by [40,41] was adopted as the primary measure for the overall quality of the model QPFs in this study, as it does not need to specify a rainfall threshold. The SSS is computed as

$$\mathrm{SSS} = 1 - \frac{\frac{1}{N}\sum_{i=1}^{N}(f_i - o_i)^2}{\frac{1}{N}\left(\sum_{i=1}^{N} f_i{}^2 + \sum_{i=1}^{N} o_i{}^2\right)}, \quad (1)$$

where f_i and o_i are the forecasted and observed rainfall amounts at the ith point, respectively, and N is the total number of verification points. Using the mean squared error (MSE), the SSS measures the overall similarity between the observed and modeled rainfall patterns against the worst possible MSE where f_i and o_i do not coexist (i.e., no overlap between the two patterns). Thus, the value of the SSS is bounded by 0 and 1, where SSS = 0 indicates the worst possible MSE and SSS = 1 means a perfect match between the two patterns.

In Section 4, where a few selected examples are presented to illustrate the control of track errors on model QPFs, traditional categorical skill scores, e.g., [58,59], are also used to assist the SSS. More specifically, the widely used threat score (TS) and bias score (BS) [60,61] are shown, and they are computed as

$$\text{TS} = H/(H + M + FA), \tag{2}$$

$$\text{BS} = (H + FA)/(H + M), \tag{3}$$

where H, M, and FA are, respectively, counts of hits, misses, and false alarms at a specified rainfall threshold among a total of N points, as obtained using a 2×2 contingency table. Thus, the TS is also bounded by 0 and 1 and gives the fraction of correct predictions of events (rainfall reaching the threshold) among all events that appear in either the observation or the model (or both). The BS gives the ratio between events in the model to those observed and therefore indicates over-prediction (BS > 1) or under-prediction (BS < 1). In practice, the BS can vary between 0 and N, and the ideal value is 1. For this calculation, a total of 15 different rainfall thresholds from 0.05 to 1000 mm (per 24 h) were used.

3. Correlation between Track Error and Model Rainfall Quality

Following the methodology described above, the skill scores of the QPFs as measured by TS and SSS were obtained for each of the 84 target days at the eight different ranges from day 1 to day 8, as were the track errors in absolute values, taken at the mid-point (1200 UTC) of the target 24 h verification periods. As the SSS can reflect the overall quality of the QPF without the need to specify a threshold, it was used to compute the correlation coefficient (R) with the track error, and the results are presented in Figure 2a–c. For this calculation, there are a total of 411 valid data pairs because a TC center may not exist or may be outside the model domain in some of the runs, rendering the track error unavailable. When all eight ranges are combined, the overall value of R is −0.559, which indicates a moderate control of the track error over the quality of the model QPF. However, as shown in [44], if only 14 target days with an observed daily rainfall of at least 350 mm were used (98 pairs), then R becomes −0.81, suggesting a much more important role played by the track error in determining the rainfall magnitude and pattern in Taiwan in more rainy cases.

When all TCs are classified into two general track types of westward-moving and northward-moving cases, the scatter plot of the SSS against track error and their R values are shown in Figure 2a. While the SSS is inversely proportional to the track error in both types, the relationship is stronger in westward-moving (R = −0.618) than in northward-moving TCs (R = −0.467). Presumably, this difference is largely because track errors in westward-moving TCs tend to influence both rainfall magnitude and pattern, while those in many northward-moving cases tend to impact only the former. For westward-moving TCs, the R value also varied to some extent depending on the track type (Figure 2b). It was the highest for those making landfall in northern and central Taiwan (track types 2 and 3, R ~ −0.687) and somewhat lower for those having a track slightly to the north (track type 1, R = −0.530) or south (track type 4, R = −0.578). However, for storms with the fifth track type, i.e., those that moved westward along the Bashi Channel to the south of Taiwan, the value of R was −0.662 and relatively high again. As the rainfall area from these TCs is mainly in eastern Taiwan, it is speculated that track errors, especially the cross-track ones, may be more important for determining the rainfall magnitude and extent in a relative sense.

If the total TC samples are grouped into those associated with southwesterly flow (sample size = 60) and those without (sample size = 351), one can see that the control of track errors over QPF quality in terms of the SSS is again much stronger in the latter group (R = −0.582) compared to the former group (R = −0.446, Figure 2c). To explore deeper into this phenomenon, a scatter plot of the SSS versus cross-track error is shown in Figure 2d, where errors to the right (left) are defined as positive (negative). Here, it is seen that the distribution of cross-track errors is somewhat skewed from a normal pattern, with more instances of rightward errors versus leftward ones. High SSS values tend to occur when cross-track errors are relatively small and vice versa and tend to be lower with larger cross-track errors. However, there are also instances of low SSS values when the cross-track errors are small, presumably with large along-track errors (so that the timing of rainfall is erroneous). There are also instances of high SSS values (≥0.5 or even ≥0.8) despite relatively large cross-track errors (≥150–200 km). In such cases, one can assume that either the TC itself played a lesser role in the production of rainfall or the model QPF happened to resemble the observation for the wrong reason, or both. From Figure 2c and some examples in past studies, e.g., [23,35,43], TCs associated with southwesterly flow can be expected to account for a higher proportion of these cases, given the lower correlation between the track error and the SSS of QPFs for them. As noted in Section 1, the detailed reasons and scenarios for decent QPFs to be produced without a good track prediction remain largely unclarified in the literature. As such issues may be best clarified through examples, several TC cases associated with southwesterly flow and certain predictions for them are used below for further exploration and discussion.

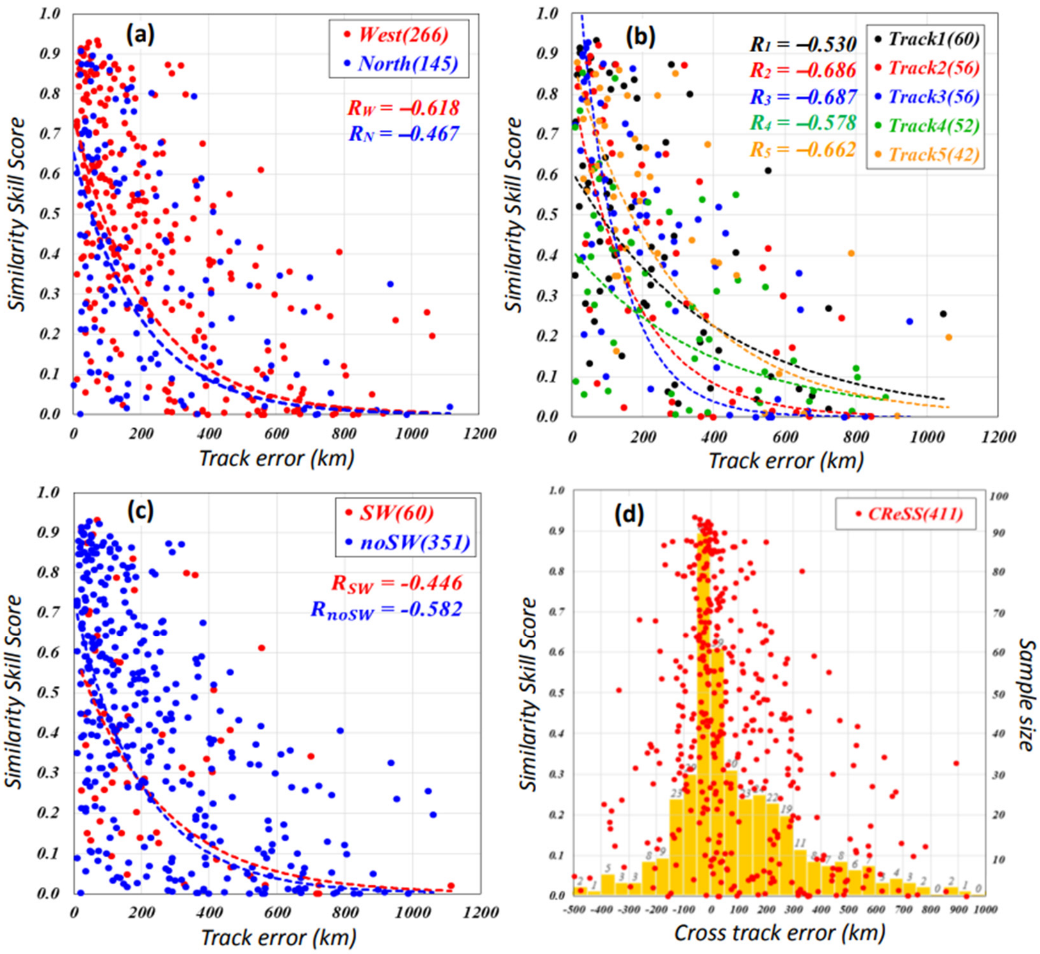

Figure 2. Scatter plots of SSS values of daily QPFs (per 24 h, 0000–2400 UTC) by the 2.5 km CReSS against track errors (km) for 24 typhoons (66 target days with an observed peak rainfall ≥ 100 mm) during 2012–2016, regardless of forecast range (days 1–8), and classified into (**a**) west-bound (red) and north-bound cases (blue), (**b**) track types 1–5 (black, red, blue, green, and orange, following the order) for the west-moving TC group, and (**c**) TCs associated with southwesterly flow (red) or not (blue), respectively. The sample size (number of days) and correlation coefficient are labeled for each group. (**d**) The scatter plot of SSS values (red dots) and distribution of sample size (orange bars) against cross-track errors (km, positive for rightward errors). For the latter, a bin width of 50 km is used for classification.

4. Examples of Typhoon Associated with Southwesterly Flow

4.1. TY Talim (2012)

In this section, a total of four typhoons are selected as examples to illustrate how QPFs with sufficient quality might (or might not) be produced when there exist relatively large track errors in the storm's position in the model. The first case is TY Talim (2012), which belongs to track type nine (Figure 1) and approaches Taiwan from the southwest. This storm reached the TS intensity near 18.5° N, 112° E in the South China Sea (SCS) at 1800 UTC 17 June and moved northeastward along the Taiwan Strait (Figure 3a). Subsequently, Talim's center passed by the shoreline of northwestern Taiwan on 20 June (in UTC) at a fast pace of about 40 km h^{-1} (Figure 3a), and its daily rainfall was concentrated mainly in the southern CMR and the southwestern plains, with a maximum of 415 mm (Figure 4a). Due to the short lifespan of Talim, only four lagged runs with TC formation were available (Figure 3a). The QPFs made on days 1 and 2 (on 19 and 20 June) were good quality, with SSS values of 0.91 and 0.79 (Figure 4a), respectively, while the two earlier runs (on 17 and 18 June) both had the TC track too far northwest and thus less ideal QPFs (SSS values of 0.30 and 0.38). However, in the run made at the longest range on day 8, in which a TC center was not identified, its QPF yielded a rather good SSS of 0.77 (Figure 4a, Table 2). Even in the two runs in the ranges of days 6 and 7, their SSS values also reached 0.7, which was not bad. In terms of categorical scores, the day-1 QPF for 20 June was obviously the best among all forecasts, with a TS reaching 0.5 at 350 mm (Figure 5a) and generally a slight over-prediction (Figure 5b), in agreement with Figure 4a. This occurred when the track errors were small (22 km at 1200 UTC, Table 2). On the other hand, the day-8 QPF made on 13 June also yielded a TS of 0.22 at 200 mm (Figure 5a, arrow), which was not achieved by any other run besides the one on day 1, also with some over-prediction (Figure 5b).

In Figure 6a, the synoptic conditions at 850 hPa associated with TY Talim (2012) at 0000 UTC 18 June are depicted, together with the movement of the storm through time. At this time, when Talim was about to start moving toward the northeast, it was seen to accompany a surge in the southwesterly flow at 850 hPa to its south. Meanwhile, another typhoon, TY Guchol (2012), was moving northward across the ocean off eastern Taiwan. Shortly afterwards, the southwesterly flow associated with both TCs merged together, and Talim started to accelerate toward the Taiwan Strait. As mentioned, the rainfall scenario from TY Talim (2012) on 20 June could be captured quite well at the short range, particularly on day 1 with the TC predicted with small track errors, as shown in Figure 7a–d that compare available TRMM PR/TMI rainrates (at 0140 and 1813 UTC, Figure 7a,b) with the CReSS prediction initialized at 0000 UTC 20 June (Figure 7c,d). In the run initialized on 13 June, despite the fact that Talim had diminished before it reached Taiwan and its center was not identifiable in the model, both the strong low-level southwesterly monsoon flow and the heavy rainfall over large areas in southern Taiwan on 20 June were still captured on day 8 (Figure 7e,f). Since the monsoon flow that was responsible for an important part of the total rainfall during Talim was captured, good QPFs were obtained (Figures 4a and 5a) even when the TC itself was not well predicted.

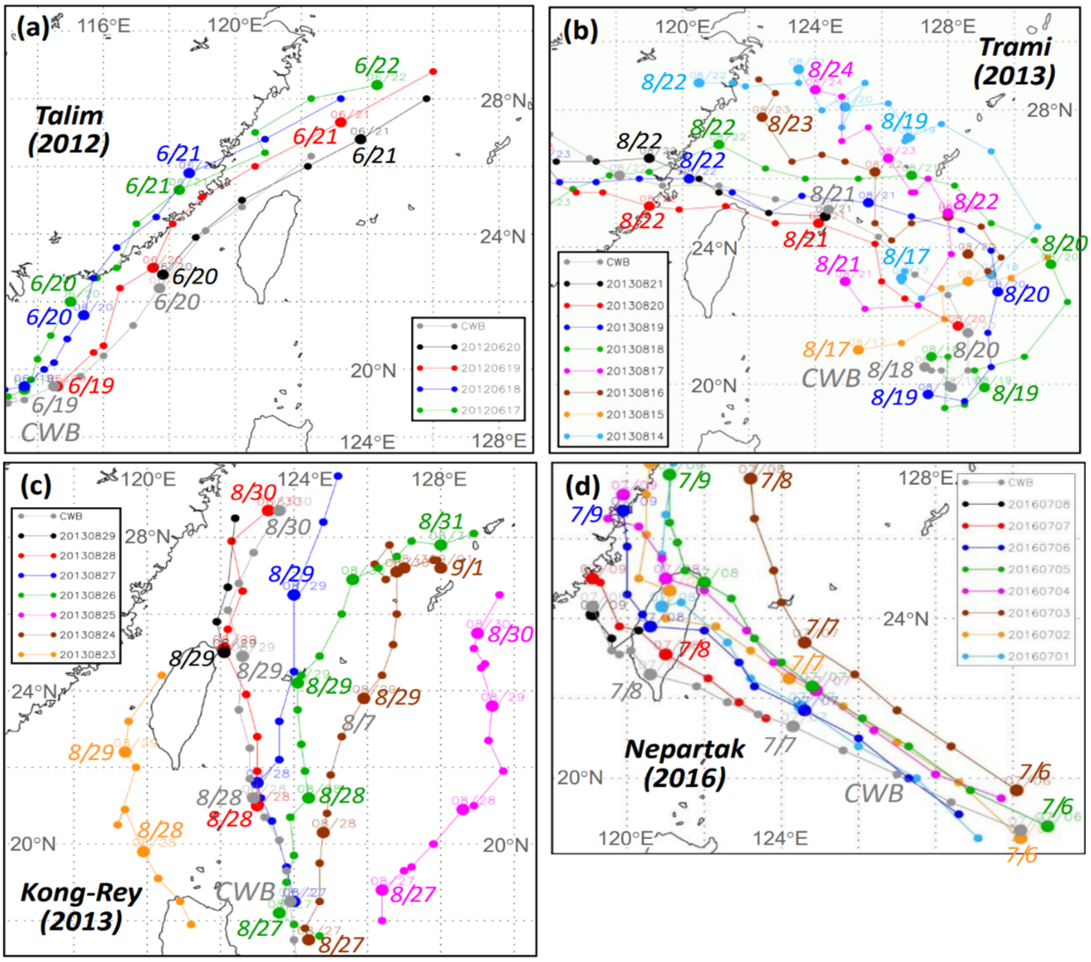

Figure 3. The CWB best track (gray, marked) and predicted tracks by the CReSS daily forecasts at 0000 UTC (colors) for TYs (**a**) Talim (2012), (**b**) Trami (2013), (**c**) Kong-Rey (2013), and (**d**) Nepartak (2016), respectively. Typhoon center positions are given every 6 h (dots), with those at 0000 UTC enlarged and labeled for month/date as needed.

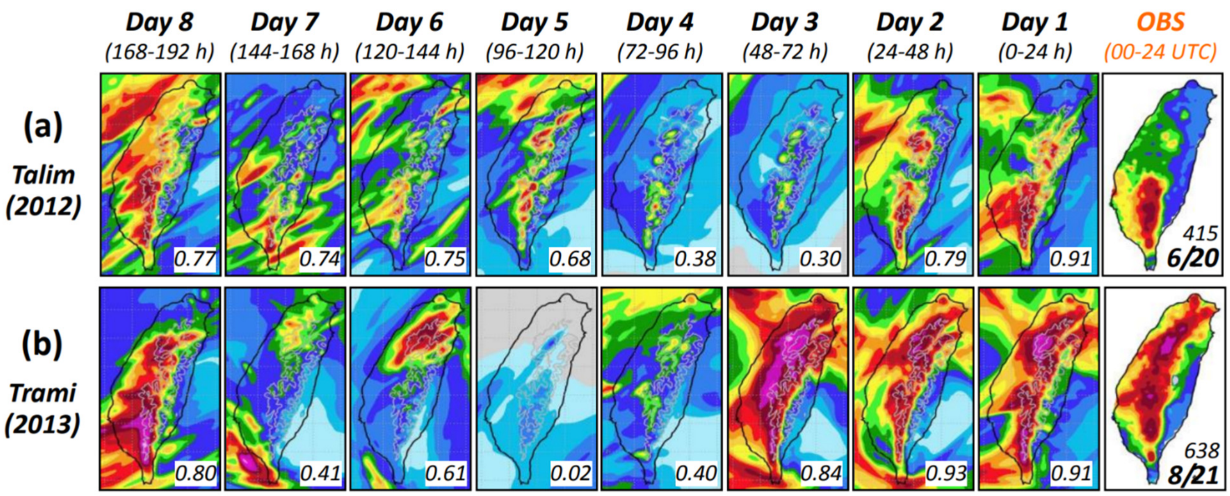

Figure 4. *Cont.*

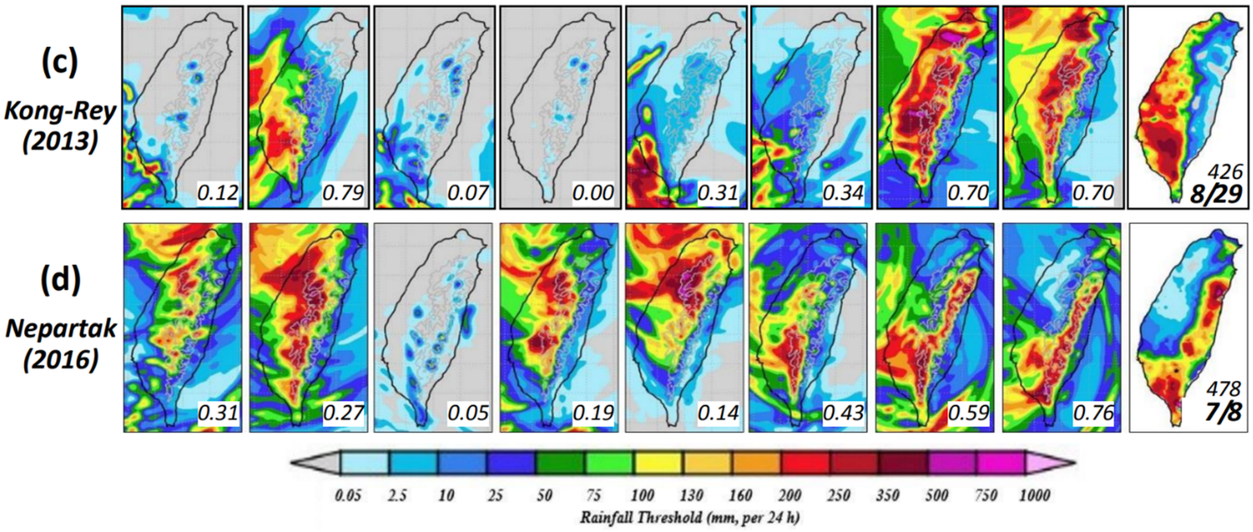

Figure 4. Model predicted (from longest to shortest range, i.e., day 8 to day 1, left to right) and observed (far right) daily rainfall (mm, 0000–2400 UTC, scale at bottom) for (**a**) 20 June for Talim (2012), (**b**) 21 August for Trami (2013), (**c**) 29 August for Kong-Rey (2013), and (**d**) 8 July for Nepartak (2016), respectively. In observation panels, the peak daily rainfall and target month/date are also labeled. In forecast panels, the SSS value for each is given (lower right).

Table 2. The four typhoons, the target days (0000–2400 UTC), observed peak daily rainfall (mm), and SSS values of QPFs and track errors (TEs; km, at 1200 UTC of target days) from daily forecasts from the shortest (day 1) to longest range (day 8) are discussed in this study. The SSS values $\geq$ 0.6 are in bold. For the TE, a symbol "#" indicates that the TC center was outside the CReSS domain, while "-" indicates the TC did not form or had dissipated in the forecast, so its center could not be located.

Typhoon Target Day Peak Rainfall		Talim 20 June 2012 415		Trami 21 August 2013 638		Kong-Rey 29 August 2013 426		Nepartak 8 July 2016 478	
SSS/TE		**SSS**	**TE**	**SSS**	**TE**	**SSS**	**TE**	**SSS**	**TE**
Forecast range	Day 1	**0.91**	22	**0.91**	22	**0.70**	45	**0.76**	23
	Day 2	**0.79**	126	**0.93**	70	**0.70**	46	0.59	78
	Day 3	0.30	408	**0.84**	175	0.34	392	0.43	168
	Day 4	0.38	435	0.40	261	0.31	321	0.14	346
	Day 5	**0.68**	#	0.02	723	0.00	717	0.19	359
	Day 6	**0.75**	#	**0.61**	553	0.07	465	0.05	884
	Day 7	**0.74**	-	0.41	461	**0.79**	358	0.27	341
	Day 8	**0.77**	-	**0.80**	332	0.12	-	0.31	408

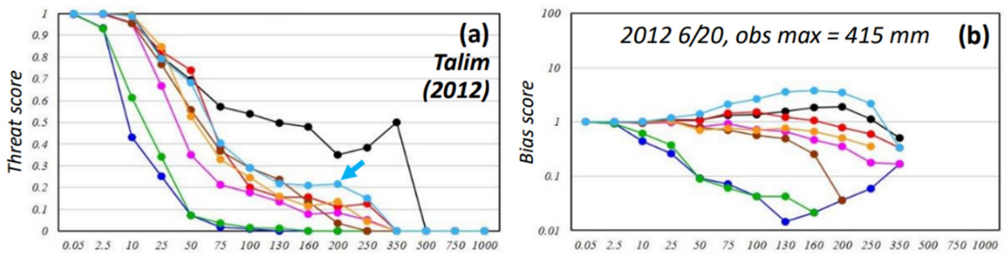

Figure 5. *Cont.*

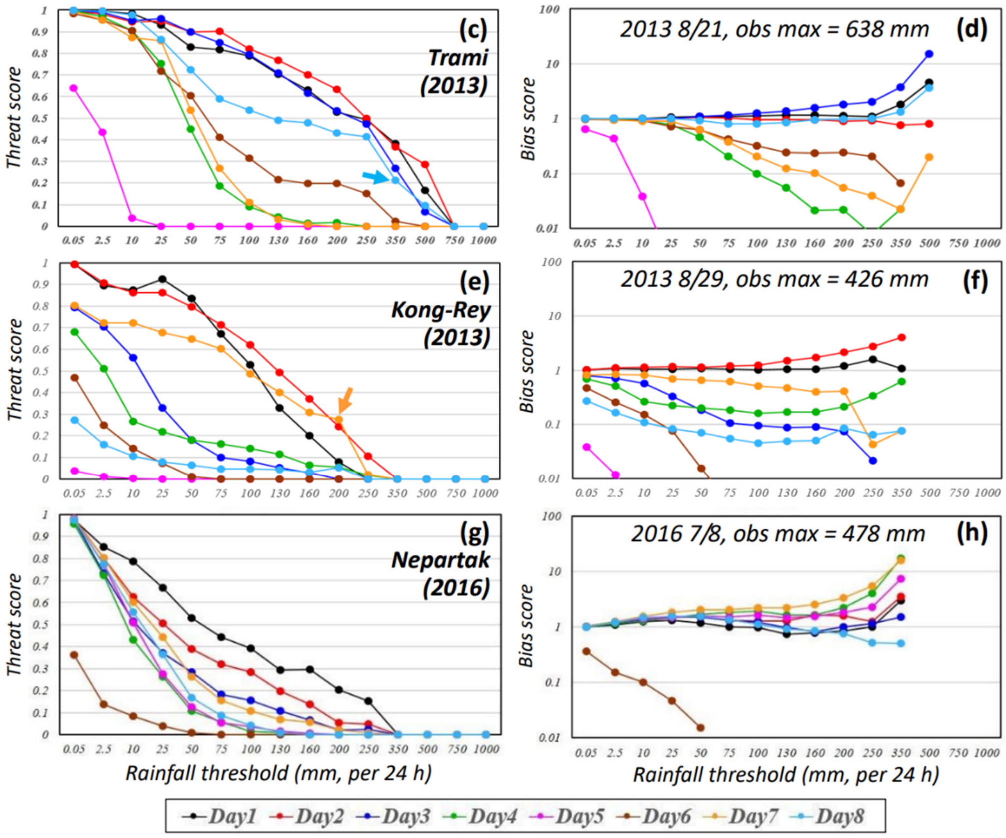

Figure 5. (**a**) TS and (**b**) BS values of 24 h QPFs made at 0000 UTC, from day 8 (longest range) to day 1 (shortest range) but all targeted for 20 June (0000–2400 UTC) for Talim (2012), at 15 thresholds from 0.05 to 1000 mm (per 24 h). (**c**–**h**) As in (**a**,**b**), but targeted for (**c**,**d**) 21 August for Trami (2013), (**e**,**f**) 29 August for Kong-Rey (2013), and (**g**,**h**) 8 July for Nepartak (2016), respectively. Arrows in (**a**,**c**,**e**) mark points beyond the short range with TS $\geq$ 0.2 at the highest threshold ($\geq$200 mm). Note that the vertical scale for BS is logarithmic.

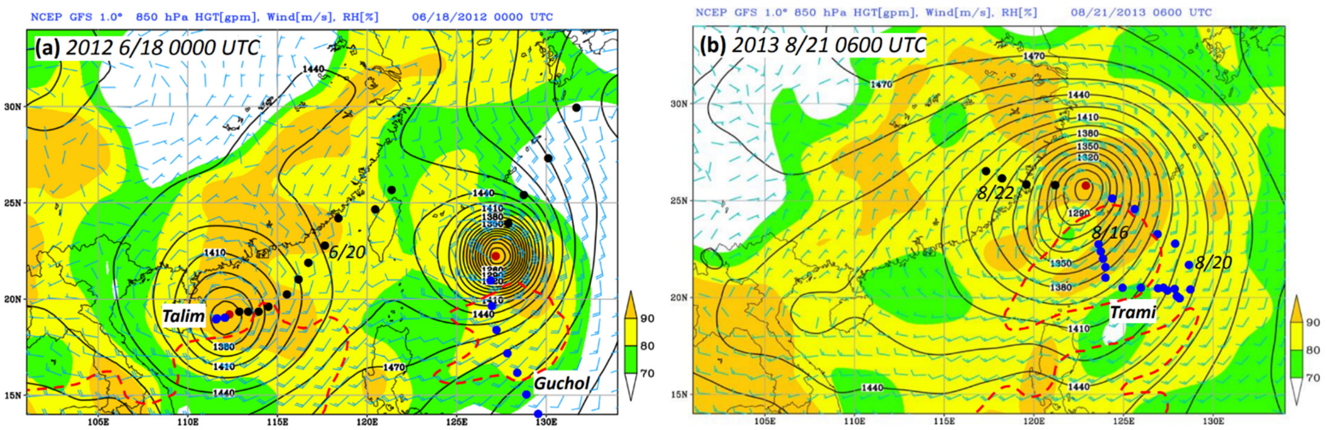

Figure 6. NCEP GFS 1° $\times$ 1° final analyses of geopotential height (gpm, contoured every 15 gpm), horizontal winds [m s^{-1}, full (half) barb = 10 (5) m s^{-1}], and relative humidity (%, color shades) at 850 hPa at (**a**) 0000 UTC 18 June during Talim (2012) and (**b**) 0600 UTC 21 August during Trami (2013). The center position of typhoon(s) of interest (name labeled) at the time of the plot is marked by a red dot, and those every 6 h before (after) are marked by blue (scarlet) dots, respectively, with month/date labeled as needed. The red dashed lines depict the areas with southwesterly winds of $\geq$20 kt.

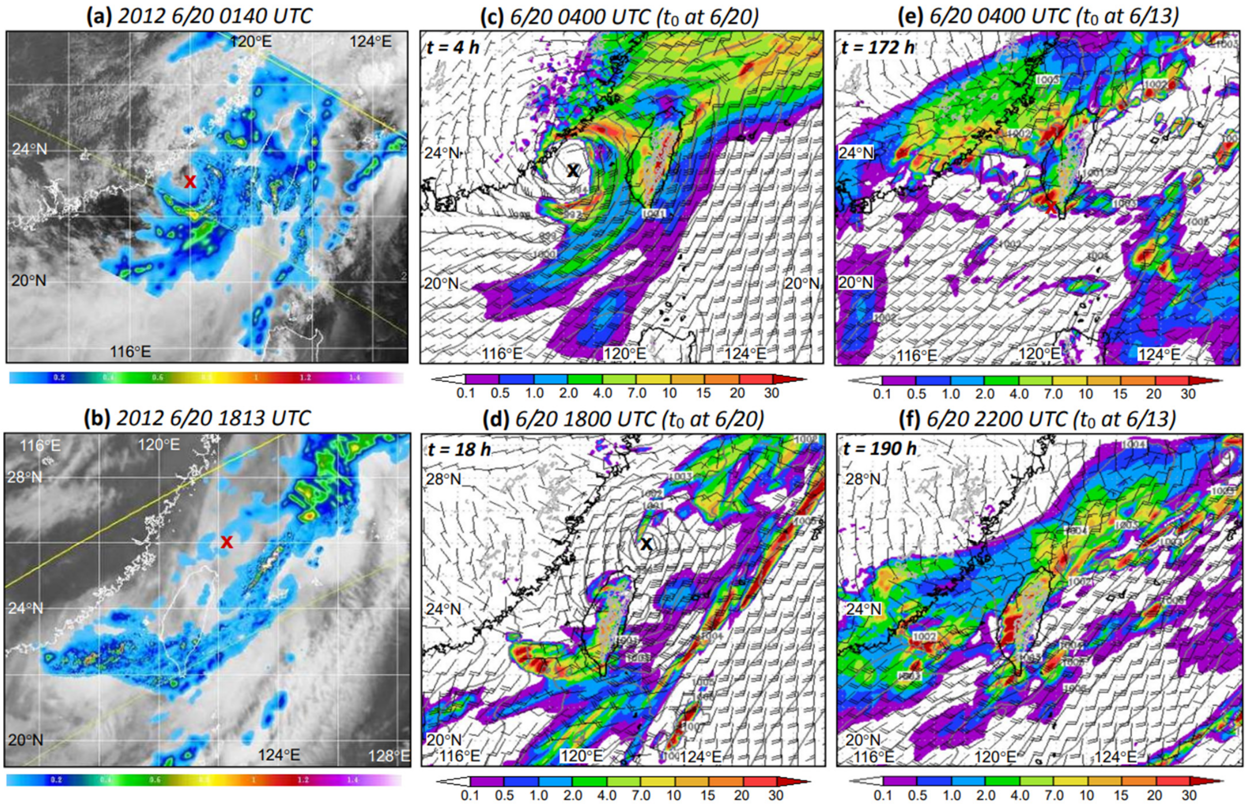

Figure 7. TRMM PR/TMI rainrates (inch h^{-1}, color), overlaid on selected cloud imagery from the geostationary satellite at closest time (source: NRL), at (**a**) 0140 and (**b**) 1813 UTC 20 June for TY Talim (2012), and model rainrates (mm h^{-1}, color) in CReSS forecast initialized on 20 June (0000 UTC), overlaid with mean sea-level pressure (hPa, ocean only) and horizontal winds (kt; 1 kt = 0.51 m s^{-1}), valid at (**c**) 0400 and (**d**) 1800 UTC 20 June 2012. The forecast time is labeled. (**e**,**f**) As in (**c**,**d**), except for the forecast initialized on 14 June and valid at (**e**) 0400 UTC (t = 172 h) and (**f**) 2200 UTC 20 June (t = 190 h), respectively. The TC centers are marked by an "x" (if present), and all panels in each row show roughly the same area with the same length scale.

4.2. TY Trami (2013)

The second case is TY Trami (2013), which had a type one track near Taiwan (Figure 3b) without a direct hit, similar to Talim. For Trami, the track errors in the daily CReSS runs were reasonably small at a short range to the target day of 21 August, although the day-3 forecast (t_0 on 19 August) also exhibited some along-track errors (about 6 h too late). Thus, quality QPFs were obtained in all three ranges on days 1–3 for Trami, with SSS values of 0.84–0.93 (Figure 4b). On longer forecast ranges, however, northward biases occurred and were, in general, larger the longer the lead time (Figure 3b). As shown in earlier studies [35,40–42] and reviewed in Section 1, the large spread in tracks from lagged runs at longer lead times due to higher forecast uncertainty, dictated by BCs from GFS forecasts, has the advantage to better ensure the coverage of the actual track. For TY Talim (2012), the QPF that had the highest SSS (=0.80) at ranges beyond 3 days was the one made on day 8, at 0000 UTC 14 August (Figure 4b), in which the track error on 21 August (at 1200 UTC) was 332 km and relatively large (also Table 2). In other runs at ranges between days 8 and 3, the SSS was at most 0.61, and one may notice that all of them also exhibited some along-track errors (timing off by at least about 15 h, see Figure 3b).

In general agreement with the SSS values, the TSs also indicated that the daily CReSS QPFs for Trami (target day on 21 August) were the best on day 2, followed by day 1, day 3, and then day 8 (Figure 5c). These four runs had TSs of 0.41–0.50 at the threshold of 250 mm (per 24 h) and 0.21–0.38 at 350 mm. The QPFs from the other runs were of lower quality and suffered under-prediction, some more serious than others (Figure 5d). Below, we discuss why the day-8 QPF for the target day of Trami (21 August) performed well, compared to those on days 4–7.

The 850-hPa synoptic conditions surrounding Taiwan at 0600 UTC 21 are shown in Figure 6b, where one can see that the pre-Trami vortex actually first appeared on 16 August just about 200 km off eastern Taiwan, then it moved slowly toward the southeast and east through 19 August. When a TC stalls in motion like this in the WNP in mid-summer, it can often interact and induce a southwesterly flow surge. Thus, when Trami passed through the ocean north of Taiwan near 21 August, it was also accompanied by strong low-level westerly and southwesterly flows, not only within its circulation but also farther south, in regions on both sides of Luzon Island (Figure 6b).

In Figure 8a,b, the TRMM PR/TMI rainrates for TY Trami (2013) at two available times, 0115 and 1748 UTC on 21 August, are shown for comparison with the model results. Again, at the short range, within day 1 for example, the center position of Trami and its associated rainfall structure could be well predicted by the 2.5 km CReSS more or less throughout the first 24 h (Figure 8c,d), resulting in high-quality QPFs for the whole day (Figures 4b and 5b). In the run that initialized on 14 August (on day 8), however, the TC position was predicted too far to the north, but such an error was mainly cross-track (Figures 3b and 8e). Under such conditions, the prevailing low-level flow was southwesterly in early 21 August in the model (Figure 8e), in contrast to the northwesterly in reality (Figures 6b and 8c). This difference resulted in too little rainfall over the SMR in the model (see Figure 4b); however, the rain over the western plains was still captured and compared quite well with the TRMM PR/TMI observations (Figure 8a,e). Later in the day when Trami's center was close to making landfall along the southeastern coast of China, the low-level prevailing winds had turned southwesterly with much rainfall on the windward side of the CMR in southern Taiwan (Figure 8d), a scenario also occurring in the run with t_0 on 14 August despite the TC being too far north (Figure 8f). Thus, in the range of day 8, the rainfall scenario for Taiwan from Trami was still correct for much of the day in the model (SSS = 0.8), although with a slight over-prediction toward the high thresholds (Figure 5d) and not enough rainfall over the SMR (Figure 4b).

4.3. TY Kong-Rey (2013)

The next case selected is TY Kong-Rey (2013), whose center moved northward off the eastern shore of Taiwan and thus belonged to track type six (Figure 3c). While both Kong-Rey (2013) and Talim (2012) were included in [35], the discussion was not from the perspective of the relationship among TE, southwesterly flow, and the quality of QPFs. In addition, the three cases were chosen because good QPFs were made at longer ranges on days 6–8 with large TEs (Figure 4 and Table 2), while there are also examples where such QPFs were made on days 4–6 at ranges in the middle but were not selected. As illustrated in [62], the rainfall accompanying Kong-Rey was largely produced through the uplift of the southwesterly flow by the CMR and was thus on the western side of Taiwan (Figure 4c), an atypical distribution for most other TCs with a track of type 6 (over eastern Taiwan). In fact, the latent heating over the island from active convection was intense and persistent enough to cause the upper-level center of Kong-Rey to shift westward and become separated from its low-level center, which was only associated with some shallow convection [62].

For Kong-Rey, the target day was 29 August 2013 at the wake of the storm, and this day was about one week after Trami and had a peak daily rainfall of 426 mm (Figure 4c). On days 1 and 2, when the track errors (for low-level center) were small (<50 km, Figure 3c), the daily rainfall distributions were reasonably predicted (Figure 4c), although the SSS values (both 0.7) were not as high as those for the first two TC cases (also Table 2). Beyond the short range on day 7, with t_0 at 0000 UTC 23 August, a high SSS of 0.79 was also obtained with much rainfall in southwestern Taiwan, despite some under-prediction (Figure 4c). This under-prediction is confirmed in Figure 5f, especially at thresholds of 250 and 350 mm. At 200 mm, however, the day-7 QPF achieved a TS of 0.28, the highest among all forecasts at this threshold (Figure 5e). Again, this good QPF was produced with a large track error

(358 km at 1200 UTC), where the model TC moved into the Taiwan Strait on 29 August (Figure 3c). In other runs where the storm tracks were too far off to the east, much less rainfall was produced in Taiwan, and the QPFs were not ideal, as expected.

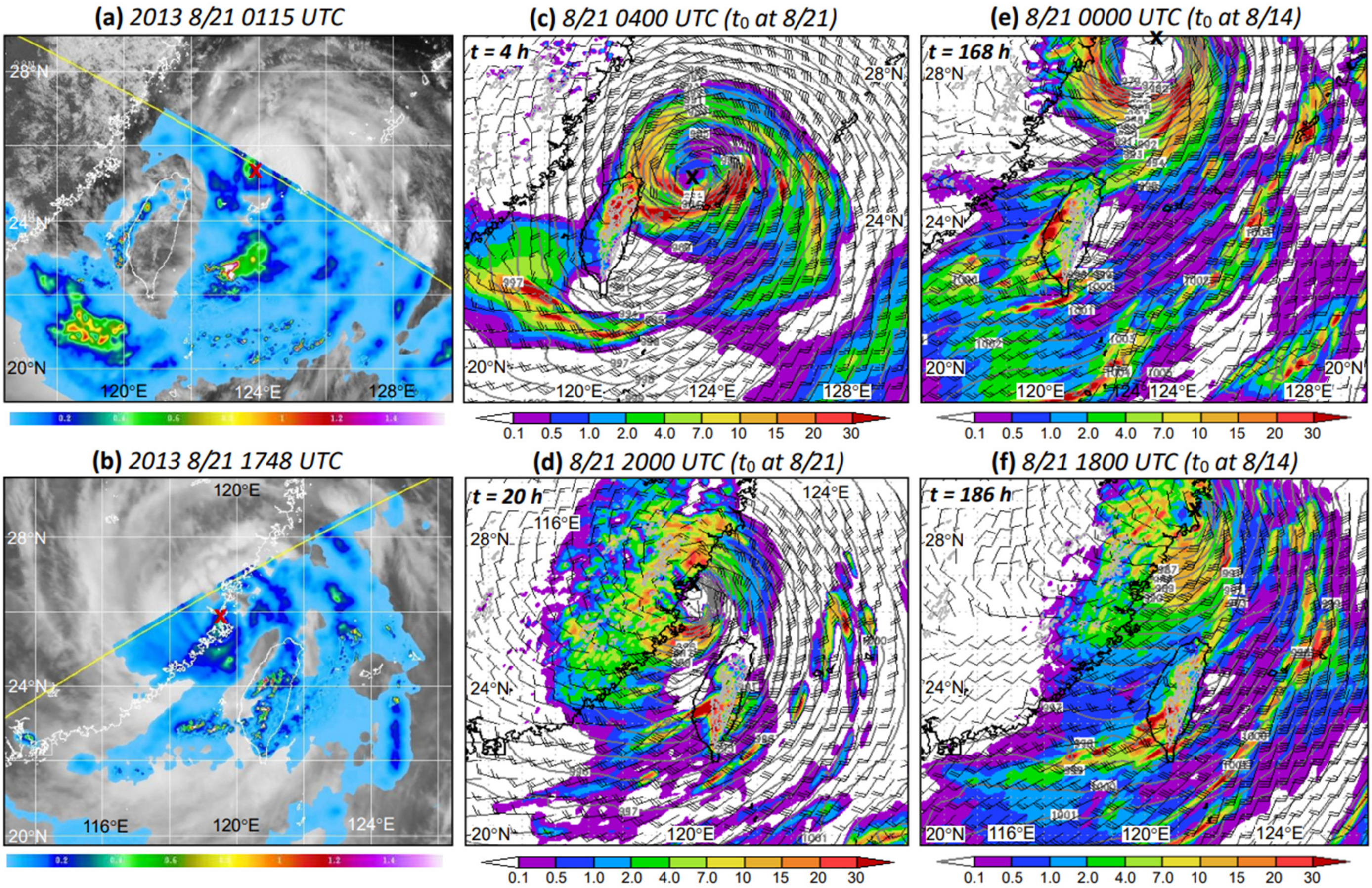

Figure 8. As in Figure 7, except for TRMM PR/TMI rainrates and satellite cloud imagery (source: NRL) at (**a**) 0115 and (**b**) 1748 UTC 21 August for TY Trami (2013), and results from the CReSS forecast initialized on 21 August and valid at (**c**) 0400 and (**d**) 2000 UTC 21 August, as well as those from the forecast initialized on 14 August and valid at (**e**) 0000 UTC (t = 168 h) and (**f**) 1800 UTC 21 August (t = 186 h), respectively.

The synoptic conditions of TY Kong-Rey (2013) at 850 hPa and 0000 UTC 29 August are shown in Figure 9a. At this time, the low-level circulation of Kong-Rey was much stronger to its south compared to its north and west, and the southwesterly flow over the northern SCS was also quite strong (≥15 kt) with high moisture (RH ≥ 80%). As the TC tracked further north on 29 August, rainfall was produced over the western side of Taiwan, as mentioned. As Kong-Rey was weakening to 990 hPa and above in its MSLP [60] and an ideal TRMM/TMI snapshot was not available on 29 August, an earlier one at 2107 UTC 28 August was selected and is shown in Figure 10a. In this figure, one can see that convection developed over southwestern Taiwan far away from the low-level center, which was associated with little convection, as described above. At the short range, these rainfall characteristics of Kong-Rey accompanying southwesterly flow could be captured to a reasonable extent, as shown in Figure 10b for t = 29 h from the run on 28 August, except perhaps some excessive rainfall in northern Taiwan (also Figure 4c). In the run initialized on 23 August, where the TC in the model erroneously moved into the Taiwan Strait, southwesterly flow also covered southwestern Taiwan and the rainfall there was roughly in the right location, i.e., west of the CMR (Figure 10c). Thus, the QPF over Taiwan made on day 7 for 29 August during Kong-Rey was also good, but apparently not for the right reason. On the other hand, in the short range when the track errors were small, the CReSS forecasts produced decent QPFs for the right reasons in all three cases, as shown by the examples (Figures 7a–d, 8a–d and 10a,b,d,e) and skill scores (Figures 4 and 5).

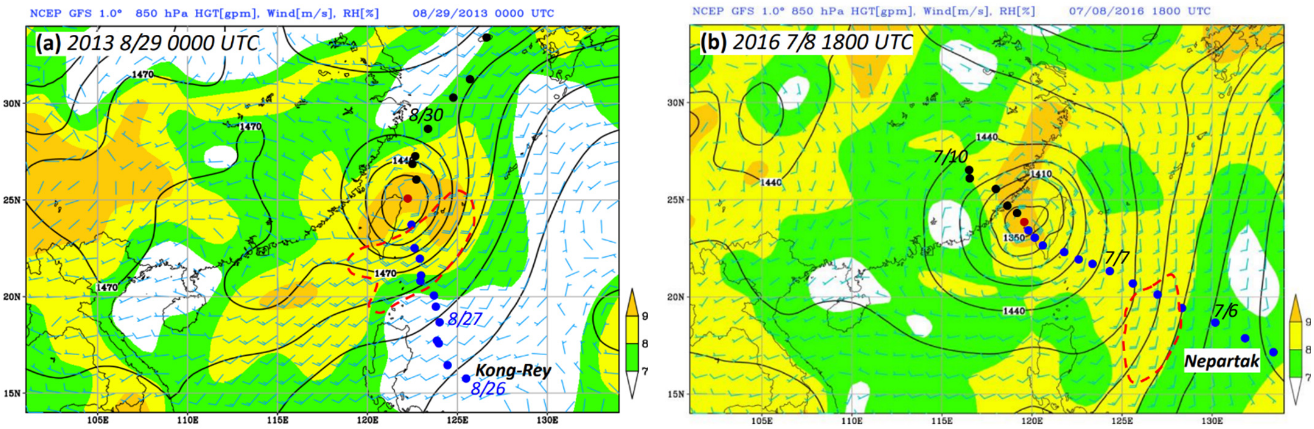

Figure 9. As in Figure 6, except at (**a**) 0000 UTC 29 August during Kong-Rey (2013) and (**b**) 0000 UTC 8 July during Nepartak (2016).

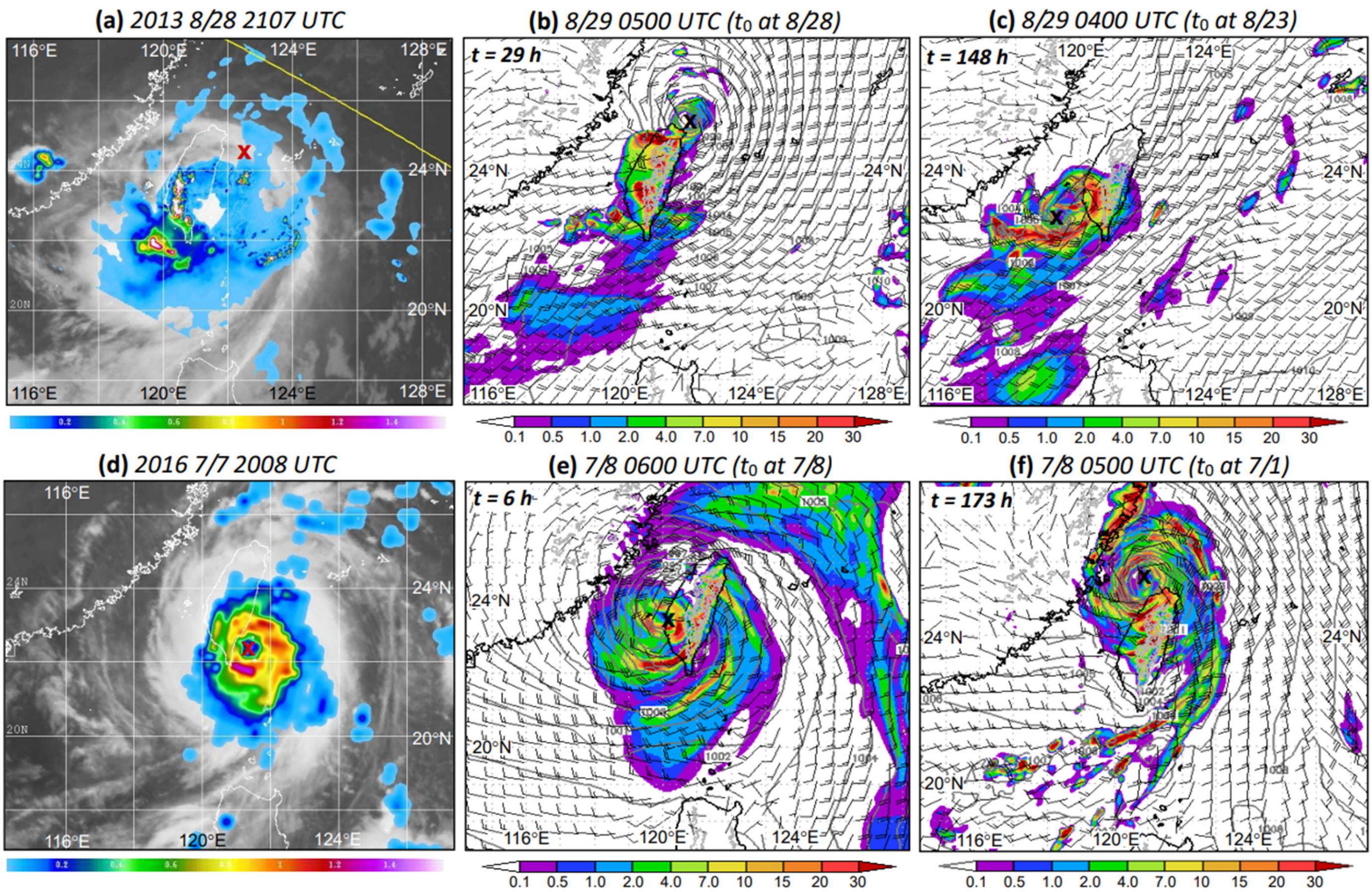

Figure 10. (**a**–**c**) As in Figure 7, except for (**a**) TRMM PR/TMI rainrates and satellite cloud imagery (source: NRL) at 2107 UTC 28 August for TY Kong-Rey (2013), and results from the CReSS forecast initialized (**b**) on 28 August and valid at 0500 UTC 29 August (t = 29 h), and (**c**) on 23 August and valid at 0400 UTC 29 August 2013 (t = 148 h). (**d**–**f**) As in (**a**–**c**), except for (**d**) TRMM/TMI and satellite observations (source: NRL) at 2008 UTC 7 July for TY Nepartak (2016), and results from the forecast initialized (**e**) on 8 July and valid at 0600 UTC 8 July (t = 6 h) and the one initialized (**f**) on 1 July and valid at 0500 UTC 8 July (t = 173 h), respectively.

4.4. TY Nepartak (2016)

Typhoon Nepartak (2016) is the final case selected for our discussion, as it was also associated with moderate southwesterly flow in its wake after passing through Taiwan. In contrast to the other three earlier TCs, however, Nepartak is a case where a quality QPF at longer lead times beyond the short range was not made, and the reasons will be the focus of the discussion below.

The observed and model-predicted tracks of TY Nepartak (2016) are depicted in Figure 3d, where one can see that this storm moved towards the west-northwest and almost penetrated the southernmost part of Taiwan (gray curve), and therefore belonged to track type five. For Nepartak, the earlier runs all exhibited a northward bias, and the track error at the landfall point did not reduce to within 150 km until day 2 (Table 2). Thus, in the forecasts on days 3–8, the predicted storm moved across the northern or central part of the island. Shown in Figure 4d, Nepartak produced much of its rainfall in the eastern and southernmost part of Taiwan. As expected, the QPFs only became better inside the short range, with SSS values of 0.43, 0.59, and 0.76 on day 3, 2, and 1, respectively (Figure 4d and Table 2). All QPFs made by earlier runs had SSS $\leq$ 0.31, but those on days 7–8 were somewhat better than those obtained on days 4–6. The TS values for Nepartak (Figure 5g) were also consistent with the SSS values, showing a TS reaching 0.2 at 200 mm only on day 1. Except on day 6, all seven runs produced at least comparable rainfall over Taiwan, so that the BS curves in Figure 5f exhibited a small spread, with a slight over-prediction towards the high thresholds in most of them.

The synoptic condition at 850 hPa associated with TY Nepartak (2016) at its wake at 1800 UTC 8 July, shortly after its center penetrated Taiwan and entered the Taiwan Strait, is depicted in Figure 9b. One can see that at this time, the TC was also associated with a southwesterly flow to its south over much of the northern SCS and surrounding Luzon, but the wind speed was only moderate at about 10 kt. In Figure 10d, a snapshot of the TRMM/TMI rainrate was also selected for TY Nepartak (2016), for the time shortly before 8 July, at 2008 UTC 7 July. At this time, the Nepartak's center was about to make landfall in southeastern Taiwan, and one can see that this storm was compact and the region of intense rainfall had a diameter of only about 300 km (Figure 10d). In the example from the day-1 forecast, valid at 0600 UTC 8 July, one can see that the structural characteristics of Nepartak were well captured, with rainfall over eastern and southern Taiwan and westerly flow prevailing over the northern SCS (Figure 10e). Well inside the short range, track errors were small in this forecast and were only 23 km at 1200 UTC (of 8 July). From the run initialized on 1 July, the prediction valid at 0500 UTC 8 July (t = 173 h) is selected in Figure 10f, where the rainfall was mostly over northern and central Taiwan, since the model TC had northward track biases and penetrated northern Taiwan then moved north instead (see Figure 3d). Thus, in this case, where the rainfall in Taiwan was caused by the circulation of Nepartak itself inside a radius of about 150–200 km from the TC center, the relatively large track errors would cause the rainfall area to be incorrect and thus low skill scores of the QPF.

5. Discussion

In Section 3, a reduced control of track error on the quality of 24 h QPFs, as reflected by the objective measure of SSS between observed and predicted rainfall patterns over Taiwan, for TCs associated with southwesterly flow ($R = -0.446$) are demonstrated, compared to those without southwesterly flow ($R = -0.582$), using the daily time-lagged CReSS forecasts for a total of 27 TCs (84 target periods) during 2012–2016. Four typhoon examples are further given in Section 4 to discuss the specific scenarios in which a quality QPF might or might not be produced, with a relatively large track error. While decent QPFs (with SSS $\geq$ 0.7) were made inside the short range for all four cases, they were also obtained on days 6–8 for TY Talim (2012), on day 8 for TY Trami (2013), and on day 7 for TY Kong-Rey (2013) with relatively large track errors ($\geq$330 km). In such forecasts, when track errors did not degrade model QPFs, there existed some common characteristics in their rainfall scenarios, i.e., all these TCs moved near or pass northern Taiwan (see Figure 3a–c), and the entire island was under the influence of strong southwesterly flow at low levels for much of the target day, despite the fact that all three TCs belong to different track types. More specific scenarios are summarized below.

For TY Talim (2012), which moved northeastward in the Taiwan Strait on 20 June (roughly from 0000 to 1500 UTC; track type nine), the day-8 QPF for this target day was used as our example (Section 4.1), with an SSS of 0.77. In this forecast, the TC had weakened to beyond identification prior to the beginning of day 8 (t = 168 h); therefore, the track error was considered large. However, its remnant remained at roughly the right location along a wind shift that passed through northern Taiwan (Figure 7). As a consequence, the southwesterly flow that produced an important part of the total rainfall over the windward slopes of Taiwan's topography was captured at a reasonable degree, and a good QPF was obtained.

For TY Trami (2013), which had a type-one track and moved from east to west just off the northern tip of Taiwan on the target day (21 August), the day-8 forecast was also used, and the TC in this run was predicted too far north (with track errors mainly in the cross-track direction). When Trami was to the east of northern Taiwan (prior to 1000 UTC), the prevailing low-level wind direction was predicted incorrectly due to the track bias (southwesterly in the model but northwesterly in reality), but in both scenarios the rain fell on the western part of the island (Figure 8c,e). Later, when Trami entered the northern Taiwan Strait, southwesterly flow prevailed over Taiwan in both the model and observation (Figure 8d,f). Therefore, despite the large northward track error, a good 24 h QPF with SSS = 0.8 was also yielded for the target day of TY Trami (2013) at the longest range on day eight, as discussed earlier in Section 4.2.

The third case of TY Kong-Rey (2013) exhibited a track of the sixth type as it moved northward off the eastern coast of Taiwan (Figure 3c). For this case, which had most daily rainfall on 29 August at its wake, the day-7 forecast produced a good daily QPF with an SSS of 0.79, even though the model storm erroneously entered the Taiwan Strait from the south (TE = 358 km). In reality, Kong-Rey was moving north on 29 August, such that Taiwan was influenced by a westerly to southwesterly flow the entire day. In the model, with the TC moving north in the Taiwan Strait, a similar south to southwesterly flow regime occurred over the southwestern part of the island where the main rainfall areas were located (Figure 10b,c). Thus, the day-7 QPF targeted for 29 August during TY Kong-Rey (2013) was also quite good, although not entirely for the right reason (Section 4.3). If the scenario in Kong-Rey is compared with that in Talim, one may find some interesting similarities between them: in Kong-Rey, the actual TC was near northern Taiwan but the model TC was in the Taiwan Strait (Figure 10), whereas the opposite occurred in Talim, i.e., the actual TC was in the Taiwan Strait but the remnant of Talim was near northern Taiwan in the forecast (Figure 7c,e).

In this study, TY Nepartak (2016) was used to provide the sole example in which the southwesterly flow was also present but without a good QPF at a longer range beyond day 3 (in fact, SSS did not reach 0.7 until day-1 forecast). The center of the westward-moving TC penetrated Taiwan at nearly its southernmost part in this case and thus belonged to the fifth track type. In Section 4.4, it is shown that because of such a track, the southwesterly flow was located too far south, and the observed rainfall was mostly from the circulation of the Nepartak itself, and thus was over eastern and southwestern Taiwan (Figure 4d). In our example of day-8 QPF, a northward bias also occurred (with a track error of 408 km), and the model rainfall was over northwestern Taiwan, and therefore was not ideal. In other words, the rainfall in Taiwan came mainly from the Nepartak itself instead of from the southwesterly flow. Subsequently, the large track error caused the QPF to degrade, with an SSS of just 0.31.

6. Concluding Remarks

Using daily QPFs over Taiwan made by the 2.5 km CReSS model during five seasons of 2012–2016, targeted for 84 days during 27 typhoons and at ranges of day one (0–24 h) to day eight (168–192 h), it is demonstrated in the present study that the control of track errors on QPF quality is reduced for typhoons associated with southwesterly flow, compared to those without. As a result, decent QPFs could still be obtained in some cases, despite relatively large track errors. Hence, the circumstances for good or bad QPFs in several selected examples are further investigated, and the reasons for the QPFs are discussed and clarified as follows.

It was found that when a southwesterly flow prevailed over much of Taiwan and contributed to a considerable amount of the total rainfall during the TC warning periods, a good QPF may still be possible with relatively large track errors if the southwesterly flow regime can be reasonably captured by the model. Such cases include TYs Talim (2012), Trami (2013), and Kong-Rey (2013). However, if much of the rainfall in Taiwan is brought by the TC circulation itself, as in the case of TY Nepartak (2016), then small track errors tend to be a prerequisite for good QPFs. Since it is quite common for typhoons to be associated with strong southwesterly flows over the WNP in the summer, and some of the most extreme rainfall events in Taiwan are produced precisely by such a type of typhoons, e.g., [4,5,23,43,63,64], a better understanding of their behaviors, as discussed in this work, can be helpful to make better use of model products and improve QPFs.

Author Contributions: Conceptualization, C.-C.W.; Formal analysis, C.-C.W. and C.-W.C.; Funding acquisition, C.-C.W. and W.-K.S.; Investigation, C.-C.W. and C.-W.C.; Data curation, C.-W.C. and C.-S.C.; Methodology, C.-C.W. and C.-W.C.; Project administration, C.-C.W. and W.-K.S.; Software, C.-W.C.; Supervision, C.-C.W.; Visualization, C.-W.C.; Writing—original draft, C.-C.W. and W.-K.S.; Writing—review and editing, all authors. All authors have read and agreed to the published version of the manuscript.

Funding: This study was supported by the National Science and Technology Council (NSTC) of Taiwan, jointly under grants MOST 111-2111-M-003-005 and MOST 111-2625-M-003-001.

Data Availability Statement: The CReSS model and its user's guide are available at http://www.rain.hyarc.nagoya-u.ac.jp/~tsuboki/cress_html/index_cress_eng.html (accessed on 10 May 2015). The NCEP GFS data are available at http://rda.ucar.edu/datasets/ds335.0/#!description (accessed on 1 November 2016), and the rainfall data are available from the CWB (https://www.cwb.gov.tw/eng/) upon request (accessed on 15 February 2017).

Acknowledgments: Valuable comments from the reviewers are appreciated. Acknowledgements also go to the NCEP for providing the GFS data that drove the CReSS forecasts, to the CWB for the rainfall data, and to the NRL for the TRMM PR/TMI imageries.

Conflicts of Interest: The authors declare no conflict of interest.

References

1. Wang, S.-T. Track, intensity, structure, wind and precipitation characteristics of typhoons affecting Taiwan. In *National Science Council of Taiwan Disaster Mitigation Research Report 80-73*; NSC 80-04140-P052-02B; Central Weather Bureau: Taipei, Taiwan, 1989; 285p. (In Chinese)
2. Kuo, Y.-H.; Chen, G.T.-J. The Taiwan Area Mesoscale Experiment (TAMEX): An overview. *Bull. Am. Meteorol. Soc.* **1990**, *71*, 488–503. [CrossRef]
3. Wu, C.-C.; Kuo, Y.-H. Typhoons affecting Taiwan: Current understanding and future challenges. *Bull. Am. Meteorol. Soc.* **1999**, *80*, 67–80. [CrossRef]
4. Fang, X.; Kuo, Y.-H.; Wang, A. The impact of Taiwan topography on the predictability of Typhoon Morakot's record-breaking rainfall: A high-resolution ensemble simulation. *Weather Forecast.* **2011**, *26*, 613–633. [CrossRef]
5. Wang, C.-C.; Kuo, H.-C.; Chen, Y.-H.; Chen, S.-H.; Tsuboki, K. A decade after Typhoon Morakot (2009): What have we learned about its physics and predictability? *Weather Forecast.* **2022**, *37*, 2161–2181. [CrossRef]
6. Li, Q.; Jia, H.; Qiu, Q.; Lu, Y.; Zhang, J.; Mao, J.; Fan, W.; Huang, M. Typhoon-induced fragility analysis of transmission towers in Ningbo area considering the effects of long-term corrosion. *Appl. Sci.* **2022**, *12*, 4774. [CrossRef]
7. Golding, B.W. Quantitative precipitation forecasting in the UK. *J. Hydrol.* **2000**, *239*, 286–305. [CrossRef]
8. Cuo, L.; Pagano, T.C.; Wang, Q.J. A review of quantitative precipitation forecasts and their use in short- to medium-range streamflow forecasting. *J. Hydrometeorol.* **2011**, *12*, 713–728. [CrossRef]
9. Toth, Z.; Kalnay, E. Ensemble forecasting at NMC: The generation of perturbations. *Bull. Am. Meteorol. Soc.* **1993**, *74*, 2317–2330. [CrossRef]

10. Mullen, S.L.; Buizza, R. Quantitative precipitation forecasts over the United States by the ECMWF ensemble prediction system. *Mon. Weather Rev.* **2001**, *129*, 638–663. [CrossRef]
11. Fritsch, J.M.; Carbone, R.E. Improving quantitative precipitation forecasts in the warm season. A USWRP research and development strategy. *Bull. Am. Meteorol. Soc.* **2004**, *85*, 955–965. [CrossRef]
12. Eckel, F.A.; Mass, C.F. Aspects of effective mesoscale, short-range ensemble forecasting. *Weather Forecast.* **2005**, *20*, 328–350. [CrossRef]
13. Wang, C.-C. The more rain, the better the model performs—The dependency of quantitative precipitation forecast skill on rainfall amount for typhoons in Taiwan. *Mon. Weather Rev.* **2015**, *143*, 1723–1748. [CrossRef]
14. Chang, C.-P.; Yeh, T.-C.; Chen, J.-M. Effects of terrain on the surface structure of typhoons over Taiwan. *Mon. Weather Rev.* **1993**, *121*, 734–752. [CrossRef]
15. Cheung, K.K.W.; Huang, L.-R.; Lee, C.-S. Characteristics of rainfall during tropical cyclone periods in Taiwan. *Nat. Hazards Earth Syst. Sci.* **2008**, *8*, 1463–1474. [CrossRef]
16. Su, S.-H.; Kuo, H.-C.; Hsu, L.-H.; Yang, Y.-T. Temporal and spatial characteristics of typhoon extreme rainfall in Taiwan. *J. Meteorol. Soc. Jpn.* **2012**, *90*, 721–736. [CrossRef]
17. Lee, C.-S.; Huang, L.-R.; Shen, H.-S.; Wang, S.-T. A climatology model for forecasting typhoon rainfall in Taiwan. *Nat. Hazards* **2006**, *37*, 87–105. [CrossRef]
18. Lee, C.-S.; Huang, L.-R.; Chen, D.Y.-C. The modification of the typhoon rainfall climatology model in Taiwan. *Nat. Hazards Earth Syst. Sci.* **2013**, *13*, 65–74. [CrossRef]
19. Hong, J.-S.; Fong, C.-T.; Hsiao, L.-F.; Yu, Y.-C.; Tzeng, C.-Y. Ensemble typhoon quantitative precipitation forecasts model in Taiwan. *Weather Forecast.* **2015**, *30*, 217–237. [CrossRef]
20. Lorenz, E.N. Deterministic nonperiodic flow. *J. Atmos. Sci.* **1963**, *20*, 130–141. [CrossRef]
21. Epstein, E.S. Stochastic dynamic prediction. *Tellus* **1969**, *21*, 739–759. [CrossRef]
22. Fang, X.; Kuo, Y.-H. Improving ensemble-based quantitative precipitation forecasts for topography-enhanced typhoon heavy rainfall over Taiwan with a modified probability-matching technique. *Mon. Weather Rev.* **2013**, *141*, 3908–3932. [CrossRef]
23. Wang, C.-C.; Kuo, H.-C.; Yeh, T.-C.; Chung, C.-H.; Chen, Y.-H.; Huang, S.-Y.; Wang, Y.-W.; Liu, C.-H. High-resolution quantitative precipitation forecasts and simulations by the Cloud-Resolving Storm Simulator (CReSS) for Typhoon Morakot (2009). *J. Hydrol.* **2013**, *506*, 26–41. [CrossRef]
24. Wang, C.-C.; Chang, C.-S.; Wang, Y.-W.; Huang, C.-C.; Wang, S.-C.; Chen, Y.-S.; Tsuboki, K.; Huang, S.-Y.; Chen, S.-H.; Chuang, P.-Y.; et al. Evaluating quantitative precipitation forecasts using the 2.5 km CReSS Model for typhoons in Taiwan: An update through the 2015 season. *Atmosphere* **2021**, *12*, 1501. [CrossRef]
25. Yang, M.-J.; Braun, S.A.; Chen, D.-S. Water budget of Typhoon Nari (2001). *Mon. Weather Rev.* **2011**, *139*, 3809–3828. [CrossRef]
26. Lin, C.-Y.; Hsu, H.-M.; Sheng, Y.-F.; Kuo, C.-H.; Liou, Y.-A. Mesoscale processes for super heavy rainfall of Typhoon Morakot (2009) over southern Taiwan. *Atmos. Chem. Phys.* **2011**, *11*, 345–361. [CrossRef]
27. Hall, J.-D.; Xue, M.; Ran, L.; Leslie, L.-M. High-resolution modeling of Typhoon Morakot (2009): Vortex Rossby waves and their role in extreme precipitation over Taiwan. *J. Atmos. Sci.* **2013**, *70*, 163–186. [CrossRef]
28. Huang, H.-L.; Yang, M.-J.; Sui, C.-H. Water budget and precipitation efficiency of Typhoon Morakot (2009). *J. Atmos. Sci.* **2014**, *71*, 112–129. [CrossRef]
29. Liu, Y.; Zhang, D.-L.; Yau, M.K. A multiscale numerical study of Hurricane Andrew (1992). Part II: Kinematics and inner-core structures. *Mon. Weather Rev.* **1999**, *127*, 2597–2616. [CrossRef]
30. Braun, S.A. A cloud-resolving simulation of Hurricane Bob (1991): Storm structure and eyewall buoyancy. *Mon. Weather Rev.* **2002**, *130*, 1573–1592. [CrossRef]
31. Clark, A.J.; Gallus, W.A.; Xue, M., Jr.; Kong, F. A comparison of precipitation forecast skill between small convection-allowing and large convection-parameterizing ensembles. *Weather Forecast.* **2009**, *24*, 1121–1140. [CrossRef]
32. Gentry, M.S.; Lackmann, G.M. Sensitivity of simulated tropical cyclone structure and intensity to horizontal resolution. *Mon. Weather Rev.* **2010**, *138*, 688–704. [CrossRef]
33. Tsuboki, K.; Sakakibara, A. Large-scale parallel computing of cloud resolving storm simulator. High Performance Computing: 4th International Symposium. In *Lecture Notes in Computer Science*; Zima, H.P., Joe, K., Sato, M., Seo, Y., Shimasaki, M., Eds.; Springer: Berlin/Heidelberg, Germany, 2002; Volume 2327, pp. 243–259.
34. Tsuboki, K.; Sakakibara, A. *Numerical Prediction of High-Impact Weather Systems: The Textbook for the Seventeenth IHP Training Course in 2007*; Hydrospheric Atmospheric Research Center, Nagoya University: Nagoya, Japan; UNESCO: Paris, France, 2007; 273p.
35. Wang, C.-C.; Huang, S.-Y.; Chen, S.-H.; Chang, C.-S.; Tsuboki, K. Cloud-resolving typhoon rainfall ensemble forecasts for Taiwan with large domain and extended range through time-lagged approach. *Weather Forecast.* **2016**, *31*, 151–172. [CrossRef]
36. Mittermaier, M.P. Improving short-range high-resolution model precipitation forecast skill using time-lagged ensembles. *Q. J. R. Meteorol. Soc.* **2007**, *133*, 1487–1500. [CrossRef]
37. Lu, C.; Yuan, H.; Schwartz, B.E.; Benjamin, S. Short-range numerical weather prediction using time-lagged ensembles. *Weather Forecast.* **2007**, *22*, 580–595. [CrossRef]
38. Yuan, H.; McGinley, J.A.; Schultz, P.J.; Anderson, C.J.; Lu, C. Short-range precipitation forecasts from time-lagged multimodel ensembles during the HMT-West-2006 campaign. *J. Hydrometeorol.* **2008**, *9*, 477–491. [CrossRef]

39. Trilaksono, N.J.; Otsuka, S.; Yoden, S. A time-lagged ensemble simulation on the modulation of precipitation over West Java in January–February 2007. *Mon. Weather Rev.* **2012**, *140*, 601–616. [CrossRef]
40. Chen, S.-H.; Wang, C.-C. Developing objective guidance for the quality of quantitative precipitation forecasts of westward-moving typhoons affecting Taiwan through machine learning. *Atmos. Sci.* **2022**, *50*, 78–125, (In Chinese with English Abstract).
41. Wang, C.-C.; Chen, S.-H.; Chen, Y.-H.; Kuo, H.-C.; Ruppert, J.H., Jr.; Tsuboki, K. Cloud-resolving time-lagged rainfall ensemble forecasts for typhoons in Taiwan: Examples of Saola (2012), Soulik (2013), and Soudelor (2015). *Weather Clim. Extrem.* **2023**, *40*, 100555. [CrossRef]
42. Wang, C.-C.; Chen, S.-H.; Chuang, P.-Y.; Chang, C.-S. Quantitative precipitation forecasts using numerical models: The example of Taiwan. In *Numerical Weather Prediction: East Asian Perspectives*; Park, S.-K., Ed.; Springer: Berlin/Heidelberg, Germany, 2023; *in press*.
43. Wang, C.-C.; Chen, S.-H.; Tsuboki, K.; Huang, S.-Y.; Chang, C.-S. Application of time-lagged ensemble quantitative precipitation forecasts for Typhoon Morakot (2009) in Taiwan by a cloud-resolving model. *Atmosphere* **2022**, *13*, 585. [CrossRef]
44. Wang, C.-C.; Chien, C.-W.; Soong, W.-K. Evaluation of eight-day typhoon quantitative precipitation forecasts in Taiwan by the 2.5-km CReSS model: Overall performance during 2012–2016 and impact of domain size. *J. Hydromet.* 2023; *under review*.
45. Wang, C.-C.; Chien, C.-W.; Chen, S.-H. Evaluation and characteristics of typhoon quantitative precipitation forecasts in Taiwan by the 2.5-km CReSS model at short and medium ranges. In Proceedings of the 2018 VOTE Meteorology Workshop, Taipei, Taiwan, 5–8 November 2018; p. 15.
46. Hsu, J. ARMTS up and running in Taiwan. *Väisälä News* **1998**, *146*, 24–26.
47. Lin, Y.-L.; Farley, R.D.; Orville, H.D. Bulk parameterization of the snow field in a cloud model. *J. Clim. Appl. Meteorol.* **1983**, *22*, 1065–1092. [CrossRef]
48. Cotton, W.R.; Tripoli, G.J.; Rauber, R.M.; Mulvihill, E.A. Numerical simulation of the effects of varying ice crystal nucleation rates and aggregation processes on orographic snowfall. *J. Clim. Appl. Meteorol.* **1986**, *25*, 1658–1680. [CrossRef]
49. Murakami, M. Numerical modeling of dynamical and microphysical evolution of an isolated convective cloud—The 19 July 1981 CCOPE cloud. *J. Meteorol. Soc. Jpn.* **1990**, *68*, 107–128. [CrossRef]
50. Ikawa, M.; Saito, K. Description of a nonhydrostatic model developed at the Forecast Research Department of the MRI. *MRI Tech. Rep.* **1991**, *28*, 238.
51. Murakami, M.; Clark, T.L.; Hall, W.D. Numerical simulations of convective snow clouds over the Sea of Japan: Two-dimensional simulation of mixed layer development and convective snow cloud formation. *J. Meteorol. Soc. Jpn.* **1994**, *72*, 43–62. [CrossRef]
52. Deardorff, J.W. Stratocumulus-capped mixed layers derived from a three-dimensional model. *Bound.-Layer Meteorol.* **1980**, *18*, 495–527. [CrossRef]
53. Kondo, J. Heat balance of the China Sea during the air mass transformation experiment. *J. Meteorol. Soc. Jpn.* **1976**, *54*, 382–398. [CrossRef]
54. Louis, J.F.; Tiedtke, M.; Geleyn, J.F. A short history of the operational PBL parameterization at ECMWF. In *Workshop on Planetary Boundary Layer Parameterization*; ECMWF: Reading, UK, 1982; pp. 59–79.
55. Segami, A.; Kurihara, K.; Nakamura, H.; Ueno, M.; Takano, I.; Tatsumi, Y. Operational mesoscale weather prediction with Japan Spectral Model. *J. Meteorol. Soc. Jpn.* **1989**, *67*, 907–924. [CrossRef]
56. Kalnay, E.; Kanamitsu, M.; Baker, W.E. Global numerical weather prediction at the National Meteorological Center. *Bull. Am. Meteorol. Soc.* **1990**, *71*, 1410–1428. [CrossRef]
57. Kleist, D.T.; Parrish, D.F.; Derber, J.C.; Treadon, R.; Wu, W.S.; Lord, S. Introduction of the GSI into the NCEP Global Data Assimilation System. *Weather Forecast.* **2009**, *24*, 1691–1705. [CrossRef]
58. Ebert, E.E.; Damrath, U.; Wergen, W.; Baldwin, M.E. The WGNE assessment of short-term quantitative precipitation forecasts (QPFs) from operational numerical weather prediction models. *Bull. Am. Meteorol. Soc.* **2003**, *84*, 481–492. [CrossRef]
59. Wilks, D.S. *Statistical Methods in the Atmospheric Sciences*, 3rd ed.; Academic Press: Cambridge, MA, USA, 2011; 704p.
60. Schaefer, J.T. The critical success index as an indicator of warning skill. *Weather Forecast.* **1990**, *5*, 570–575. [CrossRef]
61. Jolliffe, I.T.; Stephenson, D.B. *Forecast Verification: A Practitioner's Guide in Atmospheric Science*; Wiley and Sons: Hoboken, NY, USA, 2003; 240p.
62. Wang, C.-C.; Chen, Y.-H.; Li, M.-C.; Kuo, H.-C.; Tsuboki, K. On the separation of upper and low-level centres of tropical storm Kong-Rey (2013) near Taiwan in association with asymmetric latent heating. *Q. J. R. Meteorol. Soc.* **2021**, *147*, 1135–1149. [CrossRef]
63. Chien, F.-C.; Liu, Y.-C.; Lee, C.-S. Heavy rainfall and southerly flow after the leaving of Typhoon Mindulle (2004) from Taiwan. *J. Meteorol. Soc. Jpn.* **2008**, *86*, 17–44. [CrossRef]
64. Chien, F.-C.; Kuo, H.-C. On the extreme rainfall of Typhoon Morakot (2009). *J. Geophys. Res.* **2011**, *116*, D05104. [CrossRef]